Inclusive $\Sigma(1385)^{\pm}$ in 4.5 GeV p+p reactions measured in HADES

Konrad Sumara[1,*] for the HADES collaboration

[1]Faculty of Physics, Astronomy and Applied Computer Science, Jagiellonian University, Łojasiewicza 11, Kraków, Poland

Abstract. This work presents the first study of inclusive $\Sigma(1385)^{\pm}$ hyperon production in p – p collisions at a kinetic beam energy of 4.5 GeV, performed with the High-Acceptance Di-Electron Spectrometer (HADES) at GSI. The $\Sigma(1385)^{\pm}$ resonances are reconstructed via their dominant hadronic decay channels $\Sigma(1385)^{\pm} \rightarrow \Lambda(1115)\pi^{\pm}$, with subsequent $\Lambda(1115) \rightarrow p\pi^{-}$ decay.
Particle identification is based on velocity-momentum correlations and the event selection is based on time-of-flight information and topological requirements on the displaced Λ decay vertex. To further suppress combinatorial background, a weakly supervised neural network based on the Classification Without Labels method is trained directly on experimental data. The remaining background from non-Λ candidates is estimated using sideband subtraction. The $\Sigma(1385)^{\pm}$ signal within the $\Lambda\pi^{\pm}$ invariant-mass distributions is described by a relativistic Breit-Wigner function convoluted with a Gaussian resolution function on top of a smooth background. Raw $\Sigma(1385)^{\pm}$ yields are extracted differentially in transverse momentum and rapidity.
The corrections for the detector acceptance and reconstruction efficiency are obtained as a function of transverse momentum and rapidity from detailed simulations of the relevant exclusive production channels using the PLUTO event generator, with their relative contributions identified using the SMASH model.

1 Introduction

Hyperon resonances provide a sensitive probe of the dynamics of strongly interacting matter in the non-perturbative regime. Strange baryons are of particular interest, as they provide information complementary to the non-strange N and Δ states and offer a testing ground for models of hadron structure and meson-baryon interactions. The $\Sigma(1385)^{\pm}$ resonances belong to the baryon decuplet and have spin-parity $J^P = 3/2^+$. Their strong coupling to the $\Lambda\pi^{\pm}$ final state makes them experimentally accessible through their dominant hadronic decay:

$$\Sigma(1385)^{\pm} \rightarrow \Lambda\pi^{\pm} \qquad \Lambda \rightarrow p\pi^{-} \tag{1}$$

The measurements of the $\Sigma(1385)^{\pm}$ resonances in p – p collisions are very limited. An early bubble-chamber experiment at a beam momentum of 6 GeV/c [1] studied the exclusive channels $pp \rightarrow nK^{+}\Sigma(1385)^{+}$ and $pp \rightarrow pK^{0}\Sigma(1385)^{+}$. More recently, HADES has measured the exclusive $pp \rightarrow nK^{+}\Sigma(1385)^{+}$ channel at a kinetic beam energy of 3.5 GeV [2]. The

*e-mail: konrad.sumara@doctoral.uj.edu.pl

observed angular and rapidity distributions were found to be anisotropic. They were interpreted in terms of contributions involving one-pion exchange, as well as intermediate baryon resonances.

The present work extends these studies to the inclusive reconstruction of both charged states, $\Sigma(1385)^+$ and $\Sigma(1385)^-$, in p − p collisions at a kinetic beam energy of 4.5 GeV. The analysis exploits the upgraded HADES setup, in particular the Forward Detector, to increase the coverage for forward-going decay products. This analysis mainly focuses on the reconstruction and signal-extraction procedure for the two charge states, including particle identification, the hyperon selections based on specific decay topology and machine learning, as well as invariant-mass fitting. The signal yields are derived differentially as a function of the transverse momentum and the rapidity.

2 Experimental setup and event selection

The HADES experiment at GSI [3] is a fixed-target spectrometer designed for the measurement of hadron and dilepton production in nuclear collisions. The data used in this analysis were collected in February 2022 in p − p collisions with a kinetic proton beam energy of 4.5 GeV using a liquid-hydrogen target. The upgraded setup included the Forward Detector (FwDet) [4], extending the acceptance of HADES towards small polar angles to near-full phase space coverage.

The $\Sigma(1385)^{\pm}$ resonances were reconstructed through the decay chain: $\Sigma(1385)^{\pm} \rightarrow \Lambda\pi^{\pm}$, with $\Lambda \rightarrow p\pi^-$. The final decay product particles ($p\pi^-\pi^{\pm}$) are identified using momentum and time-of-flight information.

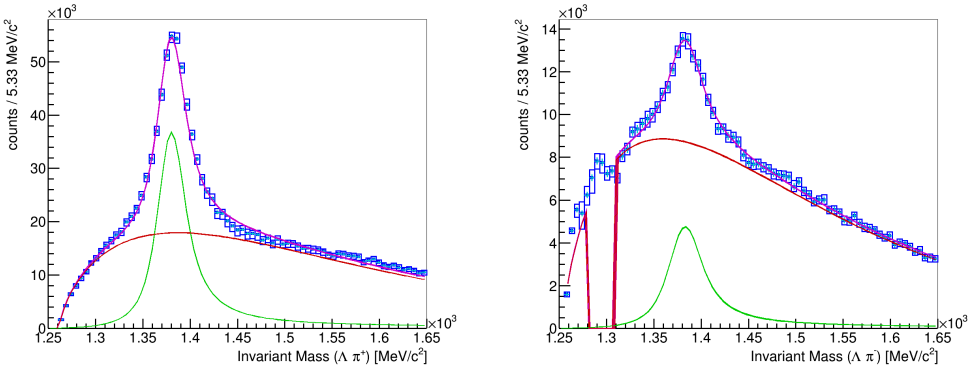
Two reconstruction configurations are considered. In the HH configuration, all three decay particles are reconstructed in the main HADES spectrometer. In the HF configuration, the pion tracks are reconstructed in HADES while the proton is detected in the Forward Detector. In FwDet, the momentum vector of the proton is determined from the track reconstructed in the straw tube tracker and the time-of-flight measured in Resistive Plate Counters. Since FwDet is located in a magnetic-field-free region, a PID hypothesis assuming proton was applied. The latter is justified by the fact that in the angular region covered by FwDet, the majority of produced particles are protons.

The Λ candidates are selected from the $p\pi^-$ pairs using displaced-vertex topology, requiring $MTD(p,\pi^-) < 20$ mm and $dist_{PV-SV} > 10$ mm, with the secondary vertex downstream of the primary vertex. The primary vertex is restricted to the target region, and one candidate per event is retained. Furthermore, a missing-mass requirement, $MM(p\pi^-\pi^{\pm}) > m_N + m_K$, suppresses incompatible channels.

The Λ(1115) selection is further improved using a weakly supervised neural-network classifier based on the Classification Without Labels (CWoLa) method [5]. The classifier is trained directly on the experimental data, using candidates from the Λ(1115) mass region as a signal-plus-background sample and candidates from mass sidebands as a background sample. The input variables contain geometrical and kinematic information describing the decay topology, including track directions, distances between tracks and vertices, and the positions of the reconstructed vertices. This approach allows the background suppression to be optimized without requiring a fully simulated signal sample.

3 Λ(1115) and $\Sigma(1385)^{\pm}$ signal extraction

After the topological and machine-learning selections, the Λ(1115) candidates are identified in the $p\pi^-$ invariant-mass distribution. The Λ signal region is defined around the mean



(a) $\Lambda\pi^+$ (b) $\Lambda\pi^-$

Figure 1: Invariant-mass distributions of the $\Lambda\pi^\pm$ candidates after sideband subtraction in the HH reconstruction configuration. The curves show the total fit, as well as its $\Sigma(1385)^\pm$ signal and background components.

mass, while the neighboring sideband regions are used to approximate the remaining non-Λ background. The $\Lambda(1115)$ peak is described by a Voigt function, with the fitted distribution providing the relative normalization of the sideband contribution.

The selected Λ candidates are combined with an additional charged pion to form $\Lambda\pi^\pm$ pairs. Before extracting the $\Sigma(1385)^\pm$ signal, the contribution of non-Λ combinations underneath the Λ peak is estimated from the sidebands. The sideband distributions are rescaled to the integral of the background contribution obtained from the Λ invariant-mass fit and subtracted from the distribution obtained in the Λ signal region. This procedure significantly reduces the combinatorial contribution while retaining the $\Sigma(1385)^\pm$ signal.

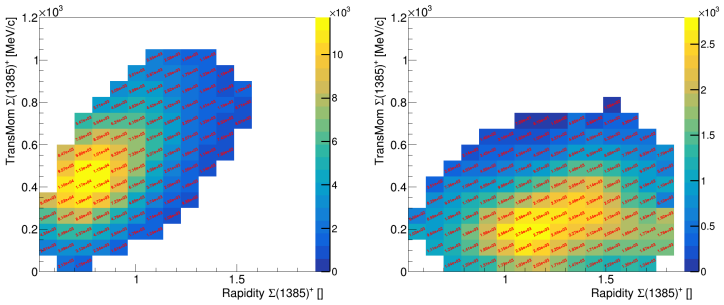
The resulting $\Lambda\pi^\pm$ invariant-mass distributions are fitted for signal extraction (see Fig. 1). The $\Sigma(1385)^\pm$ signal is described by a relativistic Breit-Wigner function with an energy-dependent width and Blatt-Weisskopf centrifugal-barrier factor, convoluted with a Gaussian resolution function. The combinatorial background is parametrized by a threshold power law multiplied by an exponential.

The $\Sigma(1385)^\pm$ signal yield is obtained through subtraction of the fitted background from the histogram in the signal region. The systematic uncertainties of the extraction are evaluated by varying the fitting range and the parameters of the sideband procedure. An additional structure around 1290 MeV/c^2 is observed in the $\Lambda\pi^-$ distribution; this region is excluded from the corresponding fit to avoid biasing the $\Sigma(1385)^-$ signal extraction.

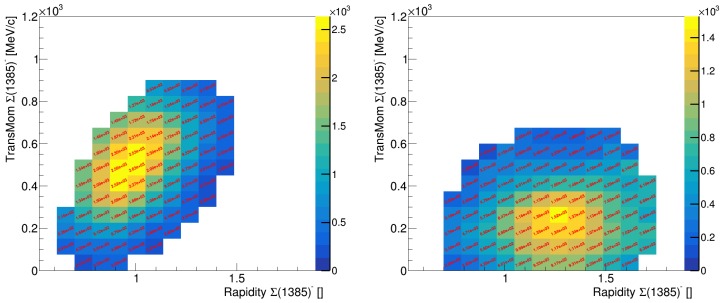
4 Raw $p_T - y$ distributions

The same signal-extraction procedure was applied differentially in the transverse momentum, p_T, and the rapidity, y. The data were divided into bins in the $p_T - y$ plane, and the complete reconstruction chain was repeated independently in each bin. The signal-extraction procedure described in Sec. 3 was repeated independently in the bins of transverse momentum p_T and rapidity y, providing the raw $\Sigma(1385)^\pm$ yield in each bin.

The two reconstruction configurations provide complementary coverage. In the HH configuration, all decay products are reconstructed in the main HADES spectrometer. In contrast, the HF configuration extends the accessible region by reconstructing the proton in the For-



(a) $\Sigma(1385)^+$



(b) $\Sigma(1385)^-$

Figure 2: The raw $\Sigma(1385)^+$ (a) and $\Sigma(1385)^-$ (b) yield reconstructed as a function of transverse momentum and rapidity before the acceptance and efficiency correction. The HH and HF configurations (left and right panels, respectively) provide complementary coverage of the kinematic phase space.

ward Detector. The resulting raw yields therefore cover a substantially larger region of the $p_T - y$ plane than would be available from the main spectrometer alone.

Figure 2 shows the resulting raw $\Sigma(1385)^{\pm}$ yield distributions before the acceptance and efficiency correction. These distributions are not corrected for detector acceptance, reconstruction efficiency, or trigger effects. Therefore, they only serve as a representation of the reconstructed signal and the kinematic coverage of the whole detector system.

5 Acceptance and efficiency correction procedure

The raw distributions described above are affected by the geometrical acceptance of HADES, detector response, reconstruction efficiency and trigger requirements. These effects are evaluated using dedicated Monte Carlo simulations.

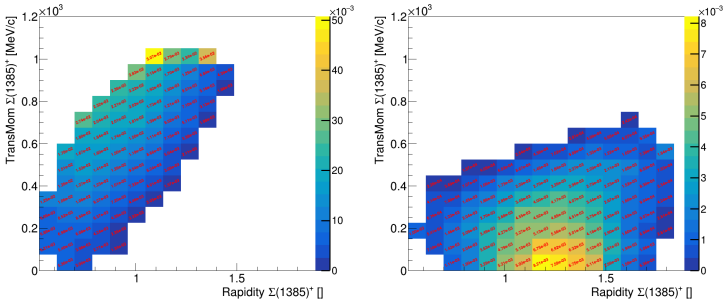
The production channels contributing to the inclusive $\Sigma(1385)^{\pm}$ production were studied with the SMASH transport model [7]. For $\Sigma(1385)^+$, 6 contributing exclusive channels were found, accounting for 99.96% of inclusive production, while for $\Sigma(1385)^-$, a single channel was found, accounting for 99.13% (see Tab. 1).

The resulting exclusive production channels were subsequently simulated with the PLUTO event generator [6], assuming uniform phase-space distributions. For $\Sigma(1385)^+$, the relevant exclusive channels were combined into a cocktail according to their relative production probabilities.

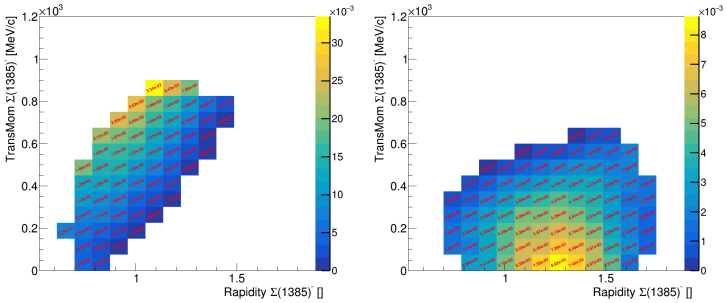
Table 1: Exclusive production channels used in the simulation and their relative contributions to inclusive $\Sigma(1385)^{\pm}$ production obtained with SMASH.

Channel	Ratio (%)
$p + p \rightarrow \Sigma(1385)^{+} + p + K^{0}$	31.89
$p + p \rightarrow \Sigma(1385)^{+} + p + K^{0} + \pi^{0}$	14.81
$p + p \rightarrow \Sigma(1385)^{+} + p + K^{+} + \pi^{-}$	15.48
$p + p \rightarrow \Sigma(1385)^{+} + n + K^{+}$	18.22
$p + p \rightarrow \Sigma(1385)^{+} + n + K^{+} + \pi^{0}$	6.80
$p + p \rightarrow \Sigma(1385)^{+} + n + K^{0} + \pi^{+}$	12.76
$p + p \rightarrow \Sigma(1385)^{-} + p + K^{+} + \pi^{+}$	99.13

The generated events were propagated through the detector simulation and reconstruction chain. The reconstructed simulated events were processed with the same particle and event selections, and invariant-mass signal-extraction procedures as the experimental data. This provides two corresponding distributions in the $p_T - y$ plane: one at the generated level in the full phase space (4π) and one after the detector acceptance and reconstruction (Reco).



(a) Correction matrix for $\Sigma(1385)^{+}$



(b) Correction matrix for $\Sigma(1385)^{-}$

Figure 3: Histograms showcasing Acceptance-and-Efficiency Correction Matrices for $\Sigma(1385)^{\pm}$ in both HH (left) and HF (right) configurations.

For each bin, the ratio of the reconstructed simulated yield to the corresponding generated yield defines the acceptance-and-efficiency response, $\epsilon(p_T, y) = \frac{N_{reco}(p_T,y)}{N_{4\pi}(p_T,y)}$. The resulting two-dimensional matrices (Fig. 3) account simultaneously for the geometrical acceptance and the losses introduced by the detector and analysis. The response was evaluated separately for

the HH and HF configurations. The dependence of the correction on the assumed production channel was investigated using the individual simulated channels; no significant channel-dependent variation of the acceptance response was observed within the studied phase space.

6 Summary and outlook

The inclusive reconstruction of $\Sigma(1385)^{\pm}$ resonances in p – p collisions at a kinetic beam energy of 4.5 GeV has been presented using data collected with the upgraded HADES detector. The resonances are reconstructed through the $\Lambda(1115)\pi^{\pm}$ decay channel, with $\Lambda(1115) \rightarrow p\pi^{-}$.

The analysis combines particle identification based on velocity–momentum correlations with displaced-vertex selections and a weakly supervised CWoLa neural-network classifier. The remaining non-Λ background is estimated using sideband subtraction, while the $\Sigma(1385)^{\pm}$ signal is extracted from the $\Lambda\pi^{\pm}$ invariant-mass distributions using a relativistic Breit-Wigner function convoluted with a Gaussian resolution function and a threshold background parametrization. The same procedure is applied differentially in p_T and rapidity to obtain raw yield distributions within the HADES acceptance.

The acceptance and reconstruction-efficiency correction procedure is based on dedicated PLUTO simulations of the relevant exclusive production channels, propagated through the detector and reconstruction chain. The resulting response matrices form the basis for determining the corrected production distributions and inclusive cross-sections. These final cross-section results, including the extrapolation to full phase space, will be presented in a dedicated publication.

The analysis framework established here also provides the basis for further studies of charged and neutral $\Sigma(1385)$ production and of the electromagnetic structure of strange baryon resonances.

References

[1] S. Klein et al., Four-Body Strange-Particle Production in pp Collisions at 6 BeV/c, Phys. Rev. D **1**, 3019 (1970), https://doi.org/10.1103/PhysRevD.1.3019

[2] G. Agakishiev et al. (HADES Collaboration), Baryonic resonances close to the $\bar{K}N$ threshold: The case of $\Sigma(1385)^{+}$ in pp collisions, Phys. Rev. C **85**, 035203 (2012), https://doi.org/10.1103/PhysRevC.85.035203

[3] G. Agakichiev et al. (HADES Collaboration), The high-acceptance dielectron spectrometer HADES, Eur. Phys. J. A **41**, 243 (2009), https://doi.org/10.1140/epja/i2009-10807-5

[4] J. Adamczewski-Musch et al. (HADES Collaboration and PANDA@HADES Collaboration), Production and electromagnetic decay of hyperons: a feasibility study with HADES as a phase-0 experiment at FAIR. Eur. Phys. J. A, **57**, 138 (2021), https://doi.org/10.48550/arXiv.2010.06961

[5] E. M. Metodiev et al., Classification without labels: learning from mixed samples in high energy physics, JHEP **10**, 174 (2017), https://doi.org/10.1007/JHEP10%282017%29174

[6] I. Fröhlich et al., Pluto: A Monte Carlo Simulation Tool for Hadronic Physics, PoS(ACAT) **076** (2007), https://doi.org/10.48550/arXiv.0708.2382

[7] J. Weil et al., Particle production and equilibrium properties within a new hadron transport approach for heavy-ion collisions, Phys. Rev. C **94**, 054905 (2016), https://doi.org/10.1103/PhysRevC.94.054905